978-1-7281-4732-1/19/$31.00 ©2019 IEEE

Automated Segmentation of Nucleus, Cytoplasm and Background of Cervical Cells from Pap-smear Images using a Trainable Pixel Level Classifier

William Wasswa (PhD)
Department of Biomedical Sciences and Engineering
Mbarara University of Science and Technology
Mbarara, Uganda
wwasswa@must.ac.ug

Johnes Obungoloch (PhD)
Department of Biomedical Sciences and Engineering
Mbarara University of Science and Technology
Mbarara, Uganda
jobungoloch@must.ac.ug

Annabella Habinka Basaza-Ejiri (PhD)
College of Computing and Engineering
St. Augustine International University
Kampala, Uganda
aejiri@saiut.ac.ug

Andrew Ware (PhD)
Faculty of Computing, Engineering and Science
University of South Wales, Prifysgol, UK
Andrew.ware@southwales.ac.uk

Abstract— Cervical cancer ranks as the fourth most prevalent cancer affecting women worldwide and its early detection provides the opportunity to help save life. Automated diagnosis of cervical cancer from pap-smear images enables accurate, reliable and timely analysis of the condition's progress. Cell segmentation is a fundamental aspect of successful automated pap-smear analysis. In this paper, a potent approach for segmentation of cervical cells from a pap-smear image into the nucleus, cytoplasm and background using pixel level information is proposed. A number of pixels from the nuclei, cytoplasm and background are extracted from 100 images to form a feature vector which is trained using noise reduction, edge detection and texture filters to produce a pixel level classifier. Comparison of the segmented images' nucleus and cytoplasm parameters (nucleus area, longest diameter, roundness, perimeter and cytoplasm area, longest diameter, roundness, perimeter) with the ground truth image features yielded average percentage errors of 0.14, 0.28, 0.03, 0.30, 0.15, 0.25, 0.05 and 0.39 respectively. Validation of the pixel classifier with 10-fold cross-validation yielded pixel classification accuracy of 98.50%, 97.70% and 98.30% with Fast Random Forest, Naïve Bayes and J48 classification methods respectively. Comparison of the segmented nucleus and cytoplasm with the ground truth nucleus and cytoplasm segmentations resulted into a Zijdenbos similarity index greater than 0.9321 and 0.9639 for nucleus and cytoplasm segmentation respectively. The results indicated that the proposed pixel level segmentation classifier was able to extract the nucleus and cytoplasm regions accurately and worked well even though there was no significant contrast between the components in the image. The results from cross-validation and test set evaluation imply that the classifier can segment cells outside the training dataset with high precision. Choosing an appropriate feature vector for training the classifier was a great challenge and a novel task in the proposed approach. As a result, good segmentation of the nucleus and cytoplasm was attained. Given the accuracy of the classifier in segmenting the nucleus, which plays an important role in cervical cancer diagnosis, the classifier can be adopted in systems for automated diagnosis of cervical cancer from pap-smear images.

Key Words— Cervix, Segmentation, Machine Learning

I. Introduction

Pap-smear screening is the most successful and effective attempt by medical science and practice to facilitate the early detection and screening of cervical cancer [1]. However, the manual analysis of the pap-smear images is time-consuming, laborious and error-prone [2]. Hundreds of sub-images within a single slide have to be examined under a microscope by a trained cytopathologist for each patient during screening. Human visual grading of microscopic biopsy images tends to be time-consuming, subjective, and inconsistent [2].

To overcome the limitations associated with the manual analysis of pap-smear images, computer-assisted pap-smear analysis systems using image processing and machine-learning techniques have been proposed. Image segmentation is a key and challenging part of such systems. Segmentation of the cervical cells acts as the foundation for all automated cervical cancer screening systems. Effective image segmentation should facilitate the extraction of meaningful information and simplification of the image data for later analysis. Moreover, poor segmentation usually leads to poor results during image analysis [3]. Most of the time, cytopathologists are interested in the evaluation of the nucleus and cytoplasm parameters to act as the basis for cell-based diagnosis screening due to the fundamentally important role of nuclei in cervical cancer cell [4]. Hence, accurate nucleus and cytoplasm segmentation are paramount. The aim of segmentation is to divide an image into several parts having similar features for easy analysis.

There are a number of image segmentation techniques but which to use depends on the dataset. Segmentation techniques can be broadly divided into two categories; (i) discontinuity based approach which looks at abrupt intensity change; and (ii) similarity-based segmentation techniques which look for image regions with similar properties [5]. Image segmentation techniques can also be classified based on the segmentation approach as described below.

1. *Thresholding techniques* where the pixels are grouped based on intensity values. These can be divided into global, variable or multiple thresholding methods [6].
2. *Edge Detection* methods where the edges are detected and then connected together to form the object boundaries to segment the required regions. These include the Gray histograms and gradient-based methods [7].
3. *Active Contours which* divide an image into multiple sub-regions of continuous boundaries [8].
4. *Region-based methods* segment the image into various regions having similar characteristics. These can be region growing or region splitting/merging methods [9].
5. *Clustering methods* segment the image into clusters having pixels with similar characteristics. These methods include hard and soft clustering methods. K-means and fuzzy c-means are the commonest hard and soft clustering mechanisms respectively [10].
6. *Trainable segmentation* which use pixel level information to train a classifier that can then be used to perform the same task on unknown data [11].

This paper presents a pixel level classifier to segment the nucleus, cytoplasm and background from cervical cells based on pixel level information and a set of training features.

II. PIXEL LEVEL BASED SEGMENTATION

Labelling data for segmentation task is difficult if compared to labelling data for classification [12]. For this reason, several weakly supervised pixel segmentation systems have been proposed in the past few years. Vezhnevets [13] proposed a method based on semantic segmentation [14]. However, the model fails to model the relationship between superpixels. To model these relationships Vezhnevets et al. [15] introduced a graphical model, named Multi-Image Model (MIM) to connect superpixels from all training images, based on their appearance similarity. Verrari et al. [16] presented a parametric family of structured pixels, where each pixel carries visual cues in a different way. An algorithm based on Gaussian processes was proposed to efficiency search the best model for different visual cues. More recently, Zhang et al. [17] proposed an algorithm that learns the distribution of spatially structural super pixel sets from image-level labels. This was achieved by first extracting graphlets from a given image. Labels from the training images were transferred into graphlets throughout a proposed manifold embedding algorithm.

In contrast with previous approaches for weakly supervised segmentation, in this paper, we avoid designing task-specific features for segmentation. Instead, a pixel level classifier learns the features and it is trained through training features which cast the problem of segmentation into the problem of finding pixel level labels from image-level labels. Another difference from our approach is that we train our classifier in different types of cervical cancer cells with the help of a skilled cytopathologist using trainable weka segmentation which has been limitedly explored for cervical cell segmentation.

III. TRAINABLE WEKA SEGMENTATION

Trainable Weka Segmentation (TWS) is an image processing toolkit that combines Fiji; an image processing toolkit developed by Schindelin et al. [18] and the state-of-the-art algorithms provided in the data mining and machine learning toolkit; Waikato Environment for Knowledge Analysis (WEKA) [19]. Trainable Weka Segmentation provides a set of library methods for extracting statistical properties of an image from user-provided pixel samples and uses that information to segment the rest of the pixels in that image (training dataset) or a similar image (testing dataset) via scripting.

Trainable Weka Segmentation has been used in a number of applications by different researchers. Dobens et al. [20] used TWS to analyze wing photomicrographs; Krueger et al. [21] used it for visualization of myocardial blood flow; and Hart et al. [22] for monitoring nests of bees. It has also been used to analyze images obtained using different imaging modalities. Kulinowski et al. [23] presented a methodology for the processing of magnetic resonance imaging data for the quantification of the dosage form matrix evolution during drug dissolution. The images were segmented into three regions using threshold-based segmentation algorithms due to the trimodal structure of the image intensity histograms. Villa et al. [24] used TWS for automated membrane segmentation in anisotropic stacks of electron microscopy brain tissue sections. The ambiguities in neuronal segmentation of a section were resolved by using the context from the neighbouring sections. Felcht et al. [25] applied TWS on confocal fluorescence microscopy images to identify a model for the opposing roles of ANG-2 in angiogenesis. Maiora et al. [26] used TWS to develop a novel active learning approach for the semi-automatic detection and segmentation of the lumen and the thrombus using image intensity features and discriminative Random Forest classifiers. Favazza et al. [27] used TWS to study the relationship between retinal and tunica vasculosa lentils (TVL) disease in retinopathy of prematurity (ROP) using angiography.

In this paper we explored its applicability in cervical cells segmentation.

IV. METHODS

The approach for the development of the proposed pixel level classifier for segmentation of the nucleus, background and cytoplasm of the cervical cells is depicted in Fig. 1.

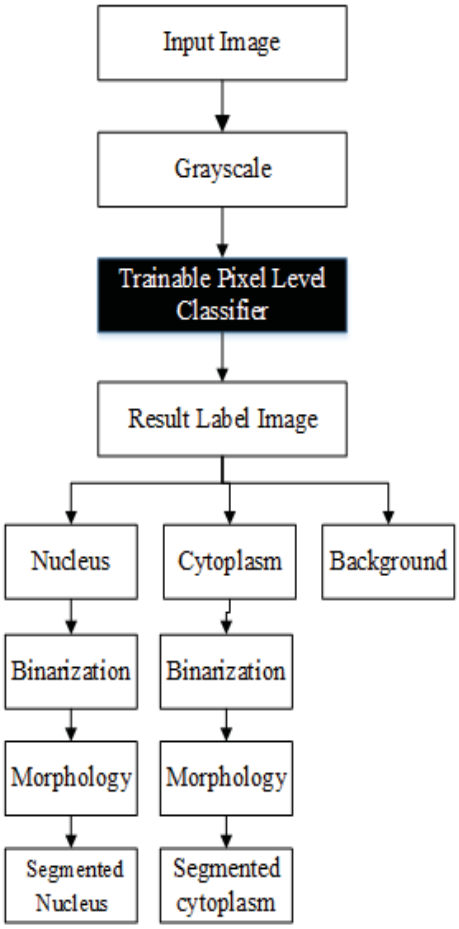

Fig.1. Nucleus, Cytoplasm and Background Segmentation

A. INPUT IMAGE

The dataset used in the work documented in this paper contains cells obtained from the Herlev Hospital Dataset (http://labs.fme.aegean.gr/decision/downloads) prepared by Jantzen et al. [28]. The dataset contains 947 cervical cells that were obtained by skilled cytotechnicians using a microscope connected to a frame grabber and taken with a resolution of 0.201µm/pixel. The images were segmented using CHAMP commercial software developed by DIMAC Imaging systems.

B. GRAYSCALE

The trainable pixel level classifier is semi-automated in the sense that the initial segmentation is carried out by an experienced cytopathologist. The cytopathologist relies on pixel level information like intensity for pixel classification. Hence grayscale conversion was carried out to ensure that the value of each pixel is a single sample representing only intensity information each pixel has. This made pixel classification easy for the cytopathologist. Conversion to grayscale was implemented using (1).

Grayscale Image= ((0.3 * R) + (0.59 * G) + (0.11 * B)). (1)

where R=Red, G=Green and B=Blue colour contributions of the new image.

C. RAINABLE PIXEL LEVEL CLASSIFIER

i. Pixel classification

The trainable pixel level classifier was developed through the steps depicted in Fig. 2. First, pixels were extracted from the nuclei, cytoplasm and background from one hundred (100) images by an experienced cytopathologist as shown in Fig. 3. Second, the selected pixels are trained using noise reduction, edge detection and texture filters to produce a pixel level classifier. Third, the pixel level classifier is cross-validated with 10-fold cross-validation.

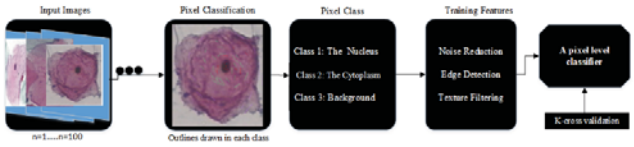

Fig.2. Pixel level classifier development stages

The pixels from the nucleus, cytoplasm and background were identified based on their physical properties which include: size, shape and intensity [29]. The nucleus is large, oval and bright. The Cytoplasm is oval and less bright whereas the background is least bright [30]. The pixels from each class (nucleus, cytoplasm and background) were used to generate a feature vector, which is defined by (2).

$$\vec{F} = \begin{bmatrix} N_i \\ C_i \\ B_i \end{bmatrix} \quad (2)$$

where N_i, C_i and B_i are the pixels from the nucleus, cytoplasm and background of the image. The feature vector information was extracted from all the one hundred images as illustrated in Fig.3.

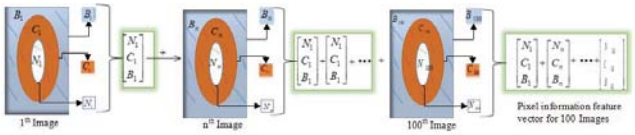

Fig.3. Generation of a feature vector from the selected pixels

ii. Training features

Each pixel extracted from the image was representing not only its intensity but a set of image features that contain a lot of information including texture, borders and colour. Choosing an appropriate feature vector for training the classifier was a great challenge and a novel task in the proposed approach. A total of 226 training features were used to train the extracted pixels shown in Table 1.

Table 1. Pixels and features used for building the classifeir

Class	Number of pixels	Number of Features
Nucleus	6,538	226
Cytoplasm	9,668	226
Background	7,928	226

The selected pixels were trained using the following training features.

Noise Reduction. The Kuwahara [31] and Bilateral filters [32] were used to train the classifier on noise removal. The bilateral filter has been reported to be an excellent filter for removing noise whilst preserving the edges [32]. The bilateral filter is defined by (3).

$$BF[I]_p = \frac{1}{w_p}\sum_{q\in s} G_{\sigma s}(\| p-q \|) G_{\sigma r}(I_p - I_q) I_q$$

where wp is the normalization factor, parameters σr and σs determine the amount of filtering of the image. In this paper, the values of 5 and 10 were used for σr and σs respectively. The Kuwahara filter was used to train the classifier on adaptive noise reduction. The filter uses linear kernels whose size is assumed to be equal to the membrane patch size of each pixel.

Edge Detection: Edge detection is a key stage in image segmentation [33]. Edge detection approaches are grouped into search-based [34] and zero-crossing based techniques. A number of boundary detection techniques have been proposed by different researchers and there is no single technique that works best for all different images [35]. In the work documented here, a Sobel filter [36], Hessian matrix [37] and Gabor filter [38] were used for training the classifier on boundary detection in any image.

Texture filtering: Texture smoothing is the method used to determine the texture colour for a texture mapped pixel, using the colours of nearby texels [39]. The mean, variance, median, maximum, minimum and entropy filters were used for texture filtering. The pixels within a region of interest in each image were subjected to the mean, variance, median, maximum and minimum operations and the target pixel set to that value. The entropy draws a circle around each pixel, gets the histogram of that split and then calculates the entropy for each pixel which acts as the basis for the pixel classification.

iii. Training the classifier

The training feature set was fed to a Fast Random Forest (FRF) classifier that trained it to build the classifier [40]. This was achieved by building a forest of classification trees using the selected pixels and the training feature set. The Random Forest Algorithm classification is shown in the pseudo-code below.

1. Randomly select *k* features from a total of *m* features where *k*<<*m*.
2. From among the *k* features, compute the node using the best split point.
3. Split the node *d* into daughter nodes using the best split.
4. Repeat steps *1* to *3* until i number of nodes has been reached.
5. Build the forest by repeating steps 1 to 4 for *n* number of times to create *n* number of trees.
6. Take the training features and use the rules of each created decision tree to predict the outcome.
7. Calculate the votes for each predicted outcome.
8. Consider the most frequently voted for the predicted outcome as the final prediction.

iv. Validation of the classifier

The accuracy of the classifier was evaluated using a 10-fold cross-validation and supplied test set using Fast Random Forest [41], Naïve Bayes [42] and J48 [43] classification models. The evaluation considered whether each pixel was correctly classified into nucleus, cytoplasm or background (True positive) or whether each pixel was incorrectly classified into the nucleus, cytoplasm or background (False positive).

D. RESULT LABEL IMAGE

The resulting image was a 3 channel image produced by applying the classifier to an input image (Fig.1). The resulting image was split into the 3 channels which corresponded to the nucleus, cytoplasm and background giving the individual segmentations for each class. These were further processed using morphology operations and image Binarization to yield better segmentation.

i. Binarization

Binarization is the process of converting a pixel image to a binary image [44]. This was import for feature extraction. The simplest way to use image binarization is to choose a threshold value, and classify all pixels with values above this threshold as white, and all other pixels as black [44]. The problem then is how to select the correct threshold for training and test images. In many cases, finding one threshold compatible with the entire dataset is very difficult, and in many cases even impossible. Therefore, adaptive local binarization was used where a window of NxN blocks slide over the entire image and threshold value is computed for each local area under the window. The method developed by Niblack et al. [45] was adopted where the threshold value for the local area under the window was calculated pixel-wise. The calculation of the threshold value was based on the local mean and standard deviation of window area. The threshold value was calculated using (4).

$$T = \mu + k * \alpha \quad (4)$$

Where μ is the mean of local area pixels of an image and α is the standard deviation of the local pixel area. The value of k=0.2 was used.

ii. Morphology

To overcome inaccuracies in the segmentation, morphological operations were carried out. Morphology is a set-theory approach that considers an image as the elements of a set and process images as geometrical shapes [46]. It is a powerful technique for solving a number of problems in image analysis and computer vision [41]. The idea is to analyze an image with a simple, predefined shape, drawing conclusions on how this shape fits or misses the shapes in the image us-

ing binary structuring elements such as crosses, squares, and open disks [47].

The two basic morphological operators are the erosion and the dilation based on Minkowski algebra [39]. In general, Dilation means objects to dilate or grow in size and erosion means the objects to shrink. The basic effect of erosion (dilation) operator on an image is to shrink (enlarge) the boundaries of foreground pixels. A dilation followed by an erosion is called a closing operation. The morphological operations can also be extended to grayscale images where the structuring element has grey values associated with every coordinate position as does the image. Dilation operation of a Grayscale image by a two-dimensional point set A is defined as;

$$(g \oplus \mathrm{A})(r,c) = \max\{g(r-k,c-l) \mid (k,l) \in A\} \quad (5)$$

Similarly, erosion of the grayscale image by a two-dimensional point set A is defined as,

$$(g \Theta \mathrm{A})(r,c) = \min\{g(r+k,c+l) \mid (k,l) \in A\} \quad (6)$$

where g is the grayscale image, A is a structuring element [40] and (*r, c*) is the pixel of the image g, (*k, l*) is the size of the element A.

In this paper, closing operation was utilized to overcome the inaccuracies in the thresholding fusing narrow breaks around the nucleus boundary and filling small holes and gaps in the image. Closing is mathematically defined as:

$$g \bullet A = [g \oplus A] \Theta A \quad (7)$$

where Θ is an erosion, $\oplus$ is a dilation and g is a binary image and A is structuring element [40]. After the morphological operation, image shape features, such as area, perimiter, roundness, longest diameter of the cytoplasm ad nucleus were extracted.

V. RESULTS

i. Pixel classification accuracy

To facilitate the evaluation of the segmentation algorithm, we first evaluated the performance of the classifier on image pixel classification. We have selected the classification accuracy as a performance measure. The accuracy is estimated by the ratio of the total number of correctly classified pixels (sum of true positives and true negatives) to the total number of pixels in the image. Other important measures are sensitivity precision, recall and F-measure. This was done with 10-fold cross-validation and test data set.

10-fold cross-validation.

Since only 100 images were used to extract 24,134 pixels used for building the classifier, cross-validation was used to estimate how the classifier was expected to perform in general when used to make predictions on data not used during its training. To reduce bias of the classifier, a larger value of k (k=10) was used. A classification accuracy of 98.5% was attained using Fast Random Forest. Detailed accuracy showing the precision, recall and F-measure per class is shown in Table 2.

Table 2. Pixel classification evaluation using Fast Random Forest

TP Rate	FP Rate	Precision	Recall	F-Measure	Accuracy	Class
0.975	0.000	1.00	0.975	0.990	0.992	Nucleus
0.993	0.012	0.979	0.994	0.987	0.982	Cytoplasm
0.981	0.011	0.985	0.981	0.983	0.981	Background
0.983	0.008	0.988	0.983	0.987	0.985	Weighted Average

The classifier's performance was also evaluated using Naïve Bayes algorithm with 10-fold cross-validation. A classification accuracy of 97.5% was obtained. Detailed accuracy by class is shown in Table 3.

Table 3. Pixel classification evaluation using Naïve Bayes

TP Rate	FP Rate	Precision	Recall	F-Measure	Accuracy	Class
0.983	0.004	0.966	0.983	0.978	0.981	Nucleus
0.965	0.042	0.947	0.965	0.954	0.973	Cytoplasm
0.954	0.013	0.966	0.959	0.937	0.976	Background
0.967	0.020	0.960	0.969	0.956	0.977	Weighted Average

Similarly, the classifier's performance was evaluated using J48 algorithm with 10-fold cross-validation. A classification accuracy of 98.3% was obtained. The detailed accuracy by class is shown in Table 4.

Table 4. Pixel classification evaluation using J48 Algorithm

TP Rate	FP Rate	Precision	Recall	F-Measure	Accuracy	Class
0.984	0.002	0.988	0.981	0.985	0.994	Nucleus
0.988	0.007	0.977	0.988	0.988	0.985	Cytoplasm
0.982	0.011	0.984	0.983	0.981	0.971	Background
0.985	0.007	0.983	0.984	0.985	0.983	Weighted Average

Test data set.

To further investigate the performance of the classifier on unseen data, it was run on a test dataset using Fast Random Forest and J48 algorithms. The dataset consisted of 817 images from the Herlev dataset that were not used to train the classifier. Classification accuracies of 98.65% and 98.99% were attained using the Fast Random Forest and the J48 Algorithms respectively.

ii. Segmentation accuracy

To evaluate the accuracy of the nucleus and cytoplasm segmentations, features were extracted from the nucleus and cytoplasm and compared with the ground truth segmentation features that were extracted using CHAMP commercial segmentation software by Jantzen et al. [28].

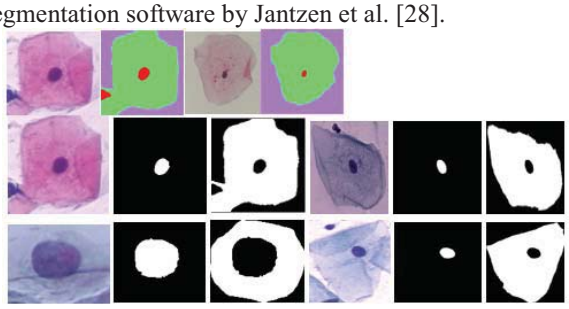

Fig. 4. Visual Analysis of the Origial Image and Segmented Images

The nucleus area, nucleus longest diameter, nucleus roundness, nucleus perimeter, cytoplasm area, cytoplasm longest diameter, cytoplasm roundness and cytoplasm perimeter were extracted from the segmented cervical cells and compared with the ground truth measurements. T he percentage errors in the nucleus area (NA), nucleus longest diameter (NLD), nucleus roundness (NR), nucleus perimeter (NP), cytoplasm area (CA), cytoplasm longest diameter (CLD), cytoplasm roundness (CR) and cytoplasm perimeter (CP) were calculated as shown in Table 5

Table 5. Percentage error between reference and extracted fetures

ID	NA	NLD	NR	NP	CA	CLD	CR	CP
1	0.07	0.18	0.08	0.16	0.18	0.19	0.05	0.42
2	0.17	0.21	0.02	0.23	0.22	0.45	0.13	0.47
3	0.12	0.15	0.01	0.41	0.17	0.48	0.08	0.23
4	0.13	0.43	0.02	0.42	0.14	0.49	0.09	0.48
5	0.17	0.23	0.03	0.39	0.19	0.15	0.05	0.54
6	0.22	0.34	0.09	0.22	0.11	0.17	0.04	0.28
7	0.15	0.32	0.02	0.31	0.12	0.31	0.01	0.38
8	0.18	0.31	0.04	0.28	0.16	0.02	0.02	0.41
9	0.07	0.28	0.06	0.32	0.12	0.17	0.02	0.41
10	0.14	0.36	0.02	0.32	0.16	0.09	0.01	0.32

A box plot was obtained to show the shape of the distribution of the percentage error, its central value, and its variability in each extracted feature as shown in Figure 5.

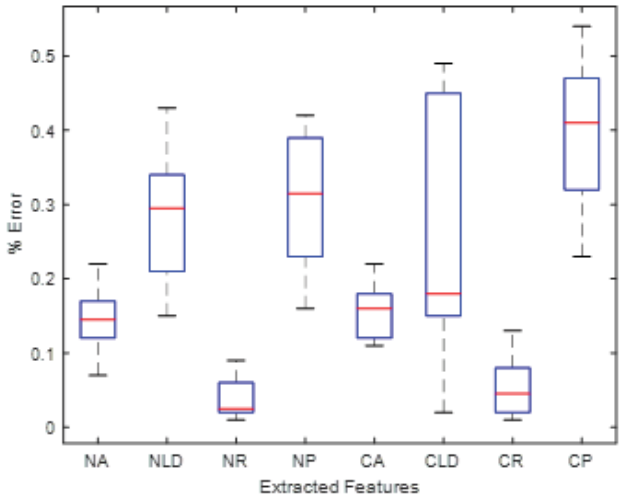

Fig. 5. Boxplot showing percentage errors in extracted features

The areas of the cytoplasm and nuclei of the segmented cervical cells were also compared with results obtained by Martin [48] and Norup [49]. The percentage errors in the areas of the nucleus (NA) and cytoplasm (CA) were calculated and shown in Table 6.

Table 6. Percentage errors in nucleus and cytoplasm Areas

	Norup [49]		Martin [48]	
ID	NA	CA	NA	CA
1	0.06	0.18	0.06	0.03
2	0.14	0.23	0.09	0.21
3	0.12	0.15	0.03	0.14
4	0.14	0.14	0.15	0.04
5	0.15	0.2	0.2	0.11
6	0.22	0.11	0.21	0.23
7	0.15	0.12	0.09	0.09
8	0.16	0.17	0.02	0.26
9	0.08	0.11	0.01	0.02
10	0.16	0.15	0.23	0.01

Our method's nucleus segmentation accuracy is compared with that of Asli et al [21] and Kuan et al. [24] who also tested their nuclei segmentation algorithm on the Herlev dataset. The same metric ZSI (Zijdenbos similarity index) is employed in this paper as used by Asli et al [21] and Kuan et al [24], and is defined by (8)

$$ZSI = 2\frac{\#\{X\, n\, Y\}}{\#\{X\}+\#\{Y\}} \qquad (8)$$

where X and Y are two sets of segmented pixels. The images in the Herlev dataset belong to 7 classes and are used to test the ability of the pixel level classifier to accurately locate nucleus regions in each class. As done in [21]and [24], we also use the segment with the highest overlap with the ground truth nucleus region for comparison. The ZSI for the pixel level classifier has a mean larger than 0.9321 and standard deviation smaller than 0.0941 for all the 7 classes, as shown in Table 7. It can be observed that a pixel level classifier performs better than that the methods by Asli et al. [21] and Kuan et al. [24].

Table 7: Comparison of the nucleus segmentation acurracy

	cells	Asli et al. [21]	Kuan et al. [24]	Pixel Level Classifier
Superficial squamous	74	0.93±0.05	0.9524±0.0013	0.9623±0.0873
Intermediate squamous	70	0.95±0.03	0.9578±0.0009	0.9529±0.0095
Columnar	98	0.90±0.07	0.9197±0.0029	**0.9321**±0.0866
Mild dysplasia	182	0.94±0.08	0.9359±0.0045	0.9395±0.0890
Moderate dysplasia	146	0.93±0.08	0.9334±0.0038	0.9469±0.0012
Severe dysplasia	197	0.92±0.10	0.9333±0.0030	0.9483±0.**0941**
Carcinoma in situ	150	0.90±0.12	0.9277±0.0039	0.9326±0.0939

Similarly, to Shys et.al [20] and Kuan et al [24] we chose 100 single-cell cervical smear images from the Herlev dataset. The performances of the pixel level classifier and the method presented in [20] and [24] are also evaluated using ZSI for cytoplasm segmentation. The statistical results are shown in Table 8.

Table 8. Comparison of the cytoplasm segmentation acurracy

Method	$\mu_{ZSI}\pm\sigma_{ZSI}$
Shys et.al [20]	0.8992±0.0348
Kuan et al [24]	0.9545±0.0439
Pixel level classifier	0.9639±0.0921

VI. DISCUSSION

The results indicated that the proposed pixel level segmentation classifier was able to extract the nucleus and cytoplasm regions accurately and worked well for the different classes of images. From the comparative analysis of the results of the segmented images' nucleus parameters (area, longest diameter, roundness and perimeter) with the ground truth measurements, it was observed that the measurements were in agreement with average percentage errors of 0.14, 0.28, 0.03 and 0.30 in each parameter respectively. Furthermore, the comparative analysis of the results of the segmented images' cytoplasm's parameters (area, longest diameter, roundness and perimeter) with the ground truth measurements, showed that the measurements were in agreement with average percentage errors of 0.15, 0.25, 0.05 and 0.39 respectively. From the results shown in Figure 4, it is ob-

served that the algorithm is excellent at nucleus segmentation. This is also shown by the least variations in the nucleus measurements shown in the boxplot and the least false positives in Table 2, Table 3 and Table 4. This could be attributed to the nucleus' brightness compared to other regions and given the fact that the developed pixel level classifier is based on pixel level information such as pixel intensity and shape. Pixel classification accuracies of 98.65% and 98.99% were obtained using the Fast Random Forest and the J48 Algorithms respectively on validation of the classifier on a test data set. This implies that the classifier can segment cells outside the training dataset with high precision. Given the accuracy of the classifier in segmenting the nucleus which plays an important role in cervical cancer diagnosis and classification, the classifier can be adapted for automated systems for cervical cancer diagnosis and classification. Comparison of the nucleus and cytoplasm segmentation with other studies showed that the pixel level classifier outcompetes them in terms of segmentation accuracy.

VII. CONCLUSSION

This paper articulates a potent approach to the segmentation of cervical cells into nucleus, cytoplasm and background using pixel level information. Choosing an appropriate feature vector for training the classifier was a great challenge and a novel task in the proposed approach. As a result, good classification accuracy in the pixel classification stage was obtained. Consequently, good segmentation of the nucleus and cytoplasm were obtained. The experimental results showed that the approach gave good pixel classification and achieved a pixel classification accuracy of 98.50%, 97.70% and 98.30% with Fast Random Forest, Naïve Bayes and J48 classifiers with 10-fold cross-validation. Comparison of the segmented nucleus and cytoplasm with the ground truth nucleus and cytoplasm segmentations resulted into a Zijdenbos similarity index of greater than 0.9321 and 0.9639 for nucleus and cytoplasm segmentation respectively. The method serves as a basis for first level segmentation of cervical cells for diagnosis and classification of cervical cancer from pap-smear images using nucleus and cytoplasm features.

ACKNOWLEDGMENT

The Authors are very grateful to African Development Bank- HEST project for providing funds for this research and the Commonwealth Scholarships for the split site scholarship at the University of Strathclyde. The support and exposure from UK greatly enhanced this research. The authors also convey their gratefulness to Mr. Abraham Birungi from Pathology department of Mbarara University of Science and Technology, Uganda for providing support with pap-images.
I would like to convey my gratefulness to Dr. Mario Giardini from the University of Strathclyde for providing support with this research while at the University of Strathclyde.

REFERENCES

[1] WHO, *Guidelines for screening and treatment of precancerous lesions for cervical cancer prevention.* 2013.

[2] E. Bengtsson and P. Malm, "Screening for cervical cancer using automated analysis of PAP-smears," *Comput. Math. Methods Med.*, 2014.

[3] C. A. Schneider, W. S. Rasband, and K. W. Eliceiri, "NIH Image to ImageJ: 25 years of image analysis," *Nature Methods*, vol. 9, no. 7. pp. 671–675, 2012.

[4] J. S. Lea and K. Y. Lin, "Cervical Cancer," *Obstetrics and Gynecology Clinics of North America*, vol. 39, no. 2. pp. 233–253, 2012.

[5] W. William, A. Ware, A. H. Basaza-Ejiri, and J. Obungoloch, "A review of image analysis and machine learning techniques for automated cervical cancer screening from pap-smear images," *Comput. Methods Programs Biomed.*, vol. 164, pp. 15–22, Oct. 2018.

[6] R. Yogamangalam and B. Karthikeyan, "Segmentation techniques comparison in image processing," *Int. J. Eng. Technol.*, 2013.

[7] R. Muthukrishnan and M. Radha, "Edge Detection Techniques for Image Segmentation.," *Int. J. Comput. Sci. ...*, vol. 3, no. 6, pp. 259–267, 2011.

[8] T. N. A. Nguyen, J. Cai, J. Zhang, and J. Zheng, "Robust interactive image segmentation using convex active contours," *IEEE Trans. Image Process.*, 2012.

[9] R. Girshick, J. Donahue, T. Darrell, and J. Malik, "Region-Based Convolutional Networks for Accurate Object Detection and Segmentation," *IEEE Trans. Pattern Anal. Mach. Intell.*, 2016.

[10] Z. W. Z. Wang and M. Y. M. Yang, "A fast clustering algorithm in image segmentation," *Comput. Eng. Technol. ICCET 2010 2nd Int. Conf.*, vol. 6, pp. V6-592-V6-594, 2010.

[11] I. Arganda-Carreras *et al.*, "Trainable Weka Segmentation: A machine learning tool for microscopy pixel classification," *Bioinformatics*, vol. 33, no. 15, pp. 2424–2426, 2017.

[12] P. O. Pinheiro and R. Collobert, "From image-level to pixel-level labeling with Convolutional Networks," in *Proceedings of the IEEE Computer Society Conference on Computer Vision and Pattern Recognition*, 2015.

[13] A. Vezhnevets and J. M. Buhmann, "Towards weakly supervised semantic segmentation by means of multiple instance and multitask learning," in *Proceedings of the IEEE Computer Society Conference on Computer Vision and Pattern Recognition*, 2010.

[14] M. A. Johnson, "Semantic segmentation and image search," 2008.

[15] W. Zhang, S. Zeng, D. Wang, and X. Xue, "Weakly supervised semantic segmentation for social

images," in *Proceedings of the IEEE Computer Society Conference on Computer Vision and Pattern Recognition*, 2015.

[16] A. Vezhnevets, V. Ferrari, and J. M. Buhmann, "Weakly supervised structured output learning for semantic segmentation," in *Proceedings of the IEEE Computer Society Conference on Computer Vision and Pattern Recognition*, 2012.

[17] L. Zhang, Y. Gao, Y. Xia, K. Lu, J. Shen, and R. Ji, "Representative discovery of structure cues for weakly-supervised image segmentation," *IEEE Trans. Multimed.*, 2014.

[18] J. Schindelin *et al.*, "Fiji: an open-source platform for biological-image analysis," *Nat. Methods*, vol. 9, no. 7, pp. 676–682, 2012.

[19] S. R. Garner, "Weka: The waikato environment for knowledge analysis," in *Proceedings of the New Zealand computer science research students conference*, 1995, pp. 57–64.

[20] A. C. Dobens and L. L. Dobens, "FijiWings: An Open Source Toolkit for Semiautomated Morphometric Analysis of Insect Wings," *G3: Genes|Genomes|Genetics*, vol. 3, no. 8, pp. 1443–1449, 2013.

[21] M. A. Krueger, S. S. Huke, and R. W. Glenny, "Visualizing regional myocardial blood flow in the mouse," *Circ. Res.*, vol. 112, no. 9, 2013.

[22] N. H. Hart and L. Huang, "Monitoring populations of solitary bees using image processing techniques," *Int. J. Comput. Appl. Technol.*, vol. 50, no. 1–2, pp. 45–50, 2014.

[23] P. Kulinowski, P. Dorozyński, A. Młynarczyk, and W. P. Węglarz, "Magnetic resonance imaging and image analysis for assessment of HPMC matrix tablets structural evolution in USP apparatus 4," *Pharm. Res.*, vol. 28, no. 5, pp. 1065–1073, 2011.

[24] V. Ljosa, K. L. Sokolnicki, and A. E. Carpenter, "Annotated high-throughput microscopy image sets for validation," *Nature Methods*, vol. 9, no. 7. p. 637, 2012.

[25] M. Felcht *et al.*, "Angiopoietin-2 differentially regulates angiogenesis through TIE2 and integrin signaling," *J. Clin. Invest.*, vol. 122, no. 6, pp. 1991–2005, 2012.

[26] J. Maiora and M. Graña, "Abdominal CTA image analisys through active learning and decision random forests: Aplication to AAA segmentation," in *Proceedings of the International Joint Conference on Neural Networks*, 2012.

[27] T. L. Favazza *et al.*, "Alterations of the tunica vasculosa lentis in the rat model of retinopathy of prematurity," *Doc. Ophthalmol.*, vol. 127, no. 1, pp. 3–11, 2013.

[28] J. Jantzen, J. Norup, G. Dounias, and B. Bjerregaard, "Pap-smear Benchmark Data For Pattern Classification," *Proc. NiSIS 2005 Nat. inspired Smart Inf. Syst.*, pp. 1–9, 2005.

[29] M. E. Plissiti and C. Nikou, "Cervical cell classification based exclusively on nucleus features," in *Lecture Notes in Computer Science (including subseries Lecture Notes in Artificial Intelligence and Lecture Notes in Bioinformatics)*, 2012, vol. 7325 LNCS, no. PART 2, pp. 483–490.

[30] P. L. Yeagle, "Cell Membrane Features," in *eLS*, 2015, pp. 1–9.

[31] K. Bartyzel, "Adaptive Kuwahara filter," *Signal, Image Video Process.*, vol. 10, no. 4, pp. 663–670, 2016.

[32] J. J. Francis and G. De Jager, "The bilateral median filter," in *SAIEE Africa Research Journal*, 2005, vol. 96, no. 2, pp. 106–111.

[33] D. Marr and E. Hildreth, "Theory of Edge Detection," *Proc. R. Soc. B Biol. Sci.*, vol. 207, no. 1167, pp. 187–217, 1980.

[34] P. F. Felzenszwalb and D. P. Huttenlocher, "Efficient graph-based image segmentation," *Int. J. Comput. Vis.*, vol. 59, no. 2, pp. 167–181, 2004.

[35] J. Canny, "A Computational Approach to Edge Detection," *IEEE Trans. Pattern Anal. Mach. Intell.*, 1986.

[36] N. Kanopoulos, N. Vasanthavada, and R. L. Baker, "Design of an Image Edge Detection Filter Using the Sobel Operator," *IEEE J. Solid-State Circuits*, vol. 23, no. 2, pp. 358–367, 1988.

[37] O. Tankyevych, H. Talbot, and P. Dokladal, "Curvilinear morpho-Hessian filter," in *2008 5th IEEE International Symposium on Biomedical Imaging: From Nano to Macro, Proceedings, ISBI*, 2008, pp. 1011–1014.

[38] D. Dunn and W. E. Higgins, "Optimal Gabor Filters for Texture Segmentation," *IEEE Trans. Image Process.*, 1995.

[39] T. Randen and J. H. Husøy, "Filtering for texture classification: A comparative study," *IEEE Trans. Pattern Anal. Mach. Intell.*, vol. 21, no. 4, pp. 291–310, 1999.

[40] L. Breiman, "Random forests," *Mach. Learn.*, 2001.

[41] M. Belgiu and L. Drăgu, "Random forest in remote sensing: A review of applications and future directions," *ISPRS Journal of Photogrammetry and Remote Sensing*. 2016.

[42] Wiki, "Naïve Bayes Classifier," *J. Eval. Clin. Pract.*, 2011.

[43] Bhargava and Sharma, "Decision Tree Analysis on J48 Algorithm for Data Mining," *Int. J. Adv. Res. Decis. Tree Anal. J48 Algorithm Data Min.*, 2013.

[44] N. Chaki, S. H. Shaikh, and K. Saeed, "Exploring image binarization techniques," *Stud. Comput. Intell.*, 2014.

[45] S. N and V. S, "Image Segmentation By Using Thresholding Techniques For Medical Images," *Comput. Sci. Eng. An Int. J.*, 2016.

[46] R. M. Haralick, S. R. Sternberg, and X. Zhuang, "Image Analysis Using Mathematical Morphology," *IEEE Trans. Pattern Anal. Mach. Intell.*, vol. 9, no. 4, pp. 532–550, 1987.

[47] T. Géraud, H. Talbot, and M. Van Droogenbroeck, "Algorithms for Mathematical Morphology," in *Mathematical Morphology: From Theory to Applications*, 2013, pp. 323–353.

[48] E. Martin, J. Jantzen, Pap-Smear Classi cation, Master's Thesis, Tech. Univ. Denmark Oersted-DTU. (2003).

[49] J. Norup, Classification of Pap-smear data by transductive neuro-fuzzy methods, Master's Thesis, Tech. Univ. Denmark Oersted-DTU. (2005) 71

A. Dr. Wasswa William has a PhD in Biomedical Engineering from Mbarara University of Science and Technology, Uganda. He has a master's in Biomedical Engineering from the University of Cape Town, South Africa. He has valuable experience in the fields of Medical Devices, Medical Imaging and Machine Learning.

B. Professor Andrew Ware is a professor in Computing at the University of South Wales. He has a lead on collaborative projects both within the UK and Europe. He has lectured in many parts of the World including the USA, Canada, Singapore and Hong Kong. His main research interest is the application of AI techniques to help solve real-world problems.

C. Assoc. Prof Annabella Habinka Basaza is an Associate professor at the College of Computing and Engineering and St. Augustine International University and in the Department of Computer Science at Mbarara University of Science and Technology. Her main research interests include ICT and Health, ICT for Education, ICT for food security, Data mining and Machine Learning.

D. Dr Johnes Obungoloch is a Biomedical Engineer with a PhD (Biomedical Engineering) from Pennsylvania State University, UK. His research interests include medical devices innovations, design and development.